Journal of Membrane Science 685 (2023) 121909

Contents lists available at ScienceDirect

Journal of Membrane Science

journal homepage: www.elsevier.com/locate/memsci

Hydrodynamics (*Reynolds number*) determine scaling, nucleation and crystal growth kinetics in membrane distillation crystallisation

A. Jikazana, P. Campo, E.J. McAdam [*]

Cranfield Water Science Institute, Cranfield University, Bedfordshire, MK43 0AL, UK

ARTICLE INFO

Keywords:
Mixing
Primary nucleation
Evaporative
Brine
Zero liquid discharge
NaCl

ABSTRACT

Reynolds number (*Re*) has been previously related to several scaling mitigation and crystallisation strategies that offer distinct hypotheses for how *Re* may regulate the kinetics of nucleation and crystal growth in membrane crystallisation. Such ambiguity has arisen from the present inability to discretely characterise induction time in membrane systems. This study therefore introduces techniques for the detection of induction time, with measurements used to develop a modified power-law relation between nucleation rate and supersaturation to establish how *Re* can be used to adjust nucleation kinetics. Increasing *Re* enhanced mass and heat transfer processes which raised permeate flux. The interfacial supersaturation set by the increase in flux, also modified the supersaturation rate at induction for crystals formed in the bulk solution, providing the first direct evidence that it is the supersaturation level set within the boundary layer which controls primary nucleation in the bulk solution. Bulk nucleation rate can therefore be adjusted in proportion to *Re*. While the extent of scaling was also determined by the interfacial supersaturation set by *Re*, its formation was shown to be more dependent on the interfacial diffusion coefficient which regulates solute backtransport and the activation energy for nucleation. Through this work we suggest that the nucleation mechanisms underlying scale formation and bulk crystallisation are distinct. The regulation of nucleation rate in the bulk solution by *Re* is described analytically through classical nucleation theory, while scaling can be mitigated through operation below a critical threshold supersaturation value that determines the rate and type of scaling that prevails. These seemingly distinct strategies can be combined through modifications to T and dT with *Re* to suppress scaling and offer refined control over the kinetics of nucleation and crystal growth.

1. Introduction

Membrane distillation crystallisation (MDC) has emerged as a promising technology for zero-liquid discharge (ZLD), the production of high value chemicals, and for resource recovery in the circular economy [1,2]. In MDC, the vapour-pressure gradient established across the hydrophobic microporous membrane fosters the selective transport of water vapour. This concentrates the feed solution to develop a supersaturated solution, after which crystallisation can proceed [1,3]. The fixed interfacial area enables the precise control of solvent transfer which advances the regulation of supersaturation. Fine regulation of supersaturation improves control over the kinetics of nucleation and crystal growth when compared to conventional crystalliser designs [4]. Temperature and concentration polarisation are also introduced by the confined laminar flow conditions to create a discrete region of elevated supersaturation within the boundary layer that forms at the membrane-solution interface [2]. Consequently, it has been postulated that nucleation and crystal growth can be independently controlled within MDC through two discrete domains: a highly supersaturated interfacial boundary layer, where nucleation is dominant, and a saturated bulk solution that primarily mediates growth [5,6]. The fully developed hydrodynamic characteristics of this supersaturated environment may therefore improve the control of crystallisation kinetics during scale-up, which is an acknowledged barrier for most existing crystallisation technologies [7].

However, the probability for inorganic scaling increases due to concentration and temperature polarisation that are set by heat and mass transfer processes local to the membrane [2]. This leads to the adhesive growth of crystals on the membrane surface and/or inside the pores, that is commonly described to proceed through a heterogeneous primary nucleation mechanism [2,8]. Scaling contributes to process failure by increasing resistance to mass and heat transfer which

---

[*] Corresponding author.
E-mail address: e.mcadam@cranfield.ac.uk (E.J. McAdam).

https://doi.org/10.1016/j.memsci.2023.121909
Received 28 March 2023; Received in revised form 13 June 2023; Accepted 4 July 2023

collectively hinder water vapour permeability [9]. Scaling has been shown to occur at low flow rates due to high concentration polarisation [10]. However, an increase in scaling rate was subsequently observed at higher flow rates where the mixing imparted within the boundary layer by higher Reynolds numbers (*Re*) has generally been assumed to mitigate such effects [11]. This complex behaviour may be related to the way in which *Re* determines the interfacial rate of heat and mass transfer, which collectively governs the permeate flux, interfacial solute concentration, and solubility constant. It is this set of interdependent parameters that ultimately inform on the supersaturation rate. The supersaturation rate determines the difference between the solubility curve and the metastable limit curve, and therefore provides the driving force for nucleation. To date, the supersaturation rate and induction time for scaling have not been characterised in membrane systems. A steep decline in permeate flux is often used as an indirect measurement of the onset of scaling, but there is general recognition that the induction time for scaling and the induction time for flux decline are phenomenologically distinct [2]. Characterisation of induction time and supersaturation rate are important since their definition can provide a complete description of the nucleation kinetics, that can relate the formation of scaling to the hydrodynamics used in membrane distillation.

It has also been proposed through modelling solute back-transport [12] that high *Re* can mitigate scaling in highly saturated solutions by ensuring that the residence time of a fluid volume at the membrane interface is shorter than the induction time required for a stable nucleus to form. However, modelling to date has been restricted to the use of empirically derived induction time and supersaturation values. This approach cannot currently account for how *Re* modifies the supersaturation rate and fluid physics within the boundary layer which will adjust these kinetically dependent parameters, therefore altering both induction time and the extent of supersaturation at induction. Without characterisation of these discrete kinetic parameters through experimental investigation, it is therefore not possible to evidence how *Re* informs crystallisation kinetics or the extent to which *Re* can be used to mitigate scaling in membrane distillation. The interfacial solute concentration, boundary-layer thickness, and interfacial diffusion coefficient also define the kinetics for crystal growth [13]. As these factors are related to the hydrodynamics adopted, the rate of growth of nucleated scale will therefore also be dependent upon the *Re* adopted. As the interfacial solute concentration at induction has not been quantified and used to accurately estimate the concentration dependent diffusion coefficient, the effects of interfacial concentration polarisation and solute back-transport on scaling are generally underestimated.

In membrane crystallisation, high *Re* are generally described as important in providing the critical shear stress required to overcome the intermolecular and frictional forces of adhesion that will lead to the detachment and recovery of crystals from the membrane [3,5,8]. This presumes a mechanism in which scaling is followed by growth with detachment achieved once a critical crystal size or a critical shear stress is achieved. However, several authors have indicated that nucleation may occur preferentially in the bulk solution (generally characterised as homogeneous primary nucleation) [14,15]. This was proposed to be the most plausible mechanism in MDC as the hydrophobicity of the membrane provides only a nominal reduction in the interfacial free energy requirement for nucleation [14]. Under such conditions, any scaling that does occur may therefore be the result of crystal deposition after undergoing primary homogeneous nucleation in the bulk solution. These mechanisms are distinct and emphasise potentially very different roles for how *Re* may moderate nucleation and crystal growth but cannot presently be elucidated as the modification of nucleation kinetics by *Re* have not been measured to date. This requires techniques to independently measure induction time in the bulk solution and at the membrane, to accommodate kinetic characterisation, and discriminate between which primary nucleation mechanism is first initiated.

This study therefore aims to provide a complete description of how *Re* governs the kinetics of nucleation and crystal growth to permit rationalisation for the selection of hydrodynamic conditions that can minimise scale and foster controlled crystal growth in the bulk solution to improve product quality, and process sustainability. To achieve this, a Nývlt-like equation for metastable zone width determination is adapted to relate boundary layer characteristics to classical nucleation theory for the first time, through the use of non-invasive techniques for the experimental derivation of induction time at the membrane and in the bulk solution. This will provide an accurate description of supersaturation rate, supersaturation and induction time to enrich primary nucleation kinetics characterisation, complemented with an enhanced description of the interfacial boundary layer with which to relate to the process of scaling and to the inception and growth of the crystal phase within the bulk solution. Specific objectives are to: (i) characterise the interfacial boundary layer to determine how the metastable zone width is adjusted when Reynolds number modifies the interfacial supersaturation rate; (ii) introduce induction time and supersaturation measured into a modified power-law description of metastability that can relate hydrodynamics to the nucleation kinetics for scaling and bulk crystallisation; (iii) compare nucleation kinetics of bulk crystallisation and scaling to determine the preference, order and dependence of these discrete phenomena; (iv) evaluate how crystal morphology is governed by the boundary layer properties set under different hydrodynamic conditions; and (v) provide an accurate description of solute backtransport based on interfacial conditions that can evidence how to suppress the onset of scaling in favour of sustained crystal growth in the bulk solution.

2. Materials and methods

2.1. Membrane distillation crystallisation experimental setup and operation

A Perspex membrane module was used to incorporate a 100 × 40 mm ePTFE flat-sheet microporous membrane comprising 0.1 μm pores (Cobetter Filtration, Hangzhou, China). The membrane was configured for direct contact, with a 0.95 mol L^{-1} sodium chloride (NaCl, 99.5%, ACROS Organics™, Fisher Chemicals, Loughborough, UK) feed solution passed counter-current to a permeate stream of deionised water (resistivity ≈15.0 MΩ cm). The feed solution *Re* was varied between 1300 and 2050 using a peristaltic pump (Watson-Marlow 530S, WMFTG, Falmouth, UK). No pulsation was evident in the feed channel within the flow rate range specified. The permeate flow rate was fixed to 65% of the feed solution. An overhead stirrer within the crystalliser vessel was set to 300 rpm (Hei-TORQUE Ultimate 400, Heidolph Instruments, Schwabach, Germany). The feed temperature at the entrance of the membrane module was maintained at 60 °C by an inline heat exchanger connected to a heater (LT ecocool 150, Grant Instruments (Cambridge) Ltd., Shepreth, UK). Inside the heat exchanger, hot water from the heater flowed counter-current to the feed solution. The permeate temperature was regulated by recirculating chiller water around the jacketed permeate vessel (LT ecocool 150, Grant Instruments (Cambridge) Ltd., Shepreth, UK). Permeate temperatures at the inlet of the membrane were varied between 35 and 45 °C to achieve temperature differences (ΔT) of 15–25 °C. Four thermocouples (EI-1034, Electronic Innovations Corporation, Colorado, USA) were inserted inline to measure entrance and exit temperatures. Conductivity of the permeate stream was monitored for salt breakthrough using an inline conductivity probe and meter (Seven2Go™ Pro S7, Mettler-Toledo Ltd, Leicester, UK). A precision balance beneath the permeate vessel recorded permeate mass over time to calculate water vapour flux (Cole Parmer Symmetry PT-4202E, Antylia Scientific, Illinois, USA).

2.2. Crystal detection and measurement

To detect bulk nucleation, an in-line turbidity probe (InPro 8200/S/Epoxy/120 turbidity sensor, Mettler-Toledo Ltd, Leicester, UK) was installed in the feed solution downstream of the membrane module and data recorded every second. The dual fibre optical sensor is an industrially proven method using backscatter technique for detecting the onset of bulk nucleation [16]. Non-invasive images of the membrane were acquired using an online digital microscope (UHM350-11 HDMI digital microscope, AmScope, UK). The digital microscope was focused on the feed side of the membrane through the Perspex cell wall and set within the maximum working distance of 145 mm. The wide-angle lens, long working distance and broad magnification range (× 20–100) permitted the full area of the membrane to be examined in real time with resolution provided by a scale equivalent to 2 μm per pixel. Consequently, while the exact moment at which a thermodynamically stable critical nucleus was formed could not be precisely determined by surface imaging (a nanometre scale event), a stable crystal phase quickly develops following induction that is readily detectable (Appendix B, Figure B1 and B2). This method is therefore analogous to widely accepted techniques for the determination of induction in solution using backscatter technique. On average NaCl crystals produced in bulk solution are around 100 μm in diameter [17]. However, scaling growth rates are extremely fast (>3 μm s^{-1}, Appendix B, Figure B3) and as such considerably larger crystals are common for scaling due to the highly supersaturated boundary layer and the progressive concentration of the feed solution. Consequently, the temporal resolution is sufficient to determine an accurate induction time for scaling, and to quantify surface area coverage. Captured images were analysed with Olympus Stream Image Analysis Software (Olympus, Southend-on-Sea, UK) and transformed into surface area coverage. For SEM analysis, crystal samples were taken from the bulk crystalliser and membrane surface 10 min after the onset of bulk nucleation. After vacuum filtration through a 0.45 μm pore nitrocellulose membrane filters (Whatman® NC45, Cytiva, Maidstone, UK), crystals were left to dry at room temperature for at least 48 h before submission for scanning electron microscopy (SEM). Crystal samples were coated by physical vapour deposition with 10 nm gold prior to analysis at an acceleration voltage, beam current and working distance of 20 keV, 300 pA and 10 mm, respectively (Tescan VEGA 4, Tescan Orsay Holding, Czech Republic).

2.3. *Introduction of revised concentration polarisation coefficient*

The concentration polarisation coefficient (CPC) is conventionally defined as [18]:

$$CPC = \frac{C_{int}}{C_b} = \exp\left(\frac{J_p}{\rho K}\right) \tag{1}$$

where C is concentration (kg m^{-3}), subscripts *int* and *b* represent the interface and bulk respectively, ρ is the solution density (kg m^{-3}), K is the mass transfer coefficient (m s^{-1}) and J_p is the permeate flux (kg m^{-2} s^{-1}):

$$J_p = \frac{\Delta m}{A_m \Delta t} \tag{2}$$

where A_m is the membrane surface area (m^2), Δm (kg) and Δt (s) are the changes in permeate mass and time, respectively. To calculate J_p, experimental data was smoothed with a 5-min average. K (m s^{-1}) was resolved using the Lévêque solution [18]:

$$K = \frac{1.62D}{d_h}\left(\frac{Vd_h^2}{DL}\right)^{\frac{1}{3}} \tag{3}$$

where D is the molecular diffusivity (m^2 s^{-1}), V is the solution velocity (m s^{-1}), d_h is the hydraulic diameter (m) and L is the membrane surface length (m). Lokare and Vidic [19] noted that this conventional analytical approach can underpredict the CPC. Hence, a more accurate determination of CPC is required to better understand the effect of *Re* on boundary-layer phenomena and the subsequent extent of scaling. Chang and Myerson [20] evidenced the concentration dependency of the diffusion coefficient within a supersaturated NaCl solution. In the conventional CPC analysis method, the diffusion coefficient is determined based on the bulk concentration, which is usually lower than the interfacial concentration due to polarisation effects. Since the diffusion coefficient of NaCl decreases drastically as supersaturation increases [20–22], this approach likely contributes to the underestimation of CPC previously observed [19]. To improve the precision of the CPC, in this study, a revised CPC value, based on the interfacial diffusion coefficient, D_{int}, was introduced. This involved initially calculating the interfacial concentration (C_{int}) applying the conventional CPC (Eq. (1)). C_{int} was then applied to empirical data to determine D_{int} (Appendix A) which was subsequently substituted into Eq. (1) to obtain the revised CPC. This revised CPC can therefore be used to improve description of solute mass transport within a supersaturated boundary layer.

2.4. *Crystallisation kinetics*

Through characterising the metastable zone width (MSZW) or maximum supersaturation level, the primary nucleation kinetics (J) of a system can be determined [18]. According to classical three-dimensional (3D) nucleation theory [22,23]:

$$J = A\exp\left(-\frac{B}{ln^2 S}\right) \tag{4}$$

where A is the pre-exponential factor, S is the supersaturation level and B is a parameter defined by:

$$B = \frac{16\pi}{3}\left(\frac{\gamma v^{\frac{2}{3}}}{k_B T}\right)^3 \tag{5}$$

γ is the interfacial energy (J m^{-2}), v is the volume of the solute molecule (m^3), k_B is the Boltzmann constant (J K^{-1}), and T is the nucleation temperature (K). Crystallisation kinetics were analysed based on the interfacial supersaturation level (S_{int}) given by:

$$S_{int} = \frac{C_{int}}{C_{int}^*} \tag{6}$$

where C_{int}^* is the interfacial saturation concentration at the interfacial temperature (kg m^{-3}). The interfacial temperature was determined iteratively based on the temperature polarisation coefficient (TPC) [18]:

$$TPC = \frac{T_{int,f} - T_{int,p}}{T_{b,f} - T_{b,p}} \tag{7}$$

where T is temperature (°C) and subscripts f and p represent the feed and permeate solutions, respectively.

$$T_{int,f} = T_{b,f} - \left(T_{b,f} - T_{b,p}\right)\left(\frac{\frac{1}{h_f}}{\frac{1}{h_f} + \frac{1}{h_p} + \frac{1}{h_c + h_v}}\right) \tag{8}$$

$$T_{int,p} = T_{b,p} + \left(T_{b,f} - T_{b,p}\right)\left(\frac{\frac{1}{h_p}}{\frac{1}{h_f} + \frac{1}{h_p} + \frac{1}{h_c + h_v}}\right) \tag{9}$$

h is the overall heat transfer coefficient for each solution, i:

$$h_i = \frac{Nuk_i}{d_h}, i = f, p \tag{10}$$

where Nu is the Nusselt number based on the Lévêque solution:

$$Nu = 0.023Re^{0.8}Pr^{\frac{1}{3}} \tag{11}$$

$$Re = \frac{\rho V d_h}{\mu} \tag{12}$$

$$Pr = \frac{c_p \mu}{k} \tag{13}$$

where μ is the dynamic viscosity (Pa s), c_p is the specific heat capacity (J kg^{-1} K^{-1}), and k is the thermal conductivity of the respective solutions (W m^{-1} K^{-1}). h_c is the conduction heat transfer coefficient:

$$h_c = \frac{k_m}{\delta_m} \tag{14}$$

δ_m is the thickness of the membrane (m) and k_m is the membrane thermal conductivity [24]:

$$k_m = \left(\frac{\varepsilon}{k_{gas}} + \frac{1-\varepsilon}{k_{solid}}\right)^{-1} \tag{15}$$

where ε is the membrane porosity, k_{gas} and k_{solid} are the thermal conductivities of the water vapour/air gas mixture and solid polymer, respectively [24]:

$$k_{gas} = 1.5x10^{-3}\sqrt{T} \tag{16}$$

$$k_{solid} = 4.86x10^{-4}T + 0.253 \tag{17}$$

h_v is the vapour heat transfer coefficient:

$$h_v = \frac{J_p \Delta H_v}{T_{int,f} - T_{int,p}} \tag{18}$$

where ΔH_v is the latent heat of vaporisation (J kg^{-1}). All solution properties were obtained from Aspen Plus software using the Elec-NRTL thermodynamic model which is suitable for highly-concentrated electrolyte solutions [25].

By assuming an empirical power law relationship between the nucleation rate and supersaturation at induction, Sangwal [23] characterised the nucleation rate, B_n (kg m^{-3} s^{-1}), using the nucleation constant, k (kg m^{-3} s^{-1}), and nucleation order, m, as follows:

$$B_n = k(lnS)^m \tag{19}$$

It can be assumed that the nucleation rate is equal to the supersaturation rate (R') at the metastable limit (the onset of nucleation) [26,23]:

$$R' = \frac{d(\Delta C_{int})}{dt}, \Delta C = C_{int} - C^*_{int} \tag{20}$$

where R' (kg m^{-3} s^{-1}) is defined as the change in interfacial supersaturation ΔC_{int} over time t. In a study by Jiang et al. [26], R' was equated to the concentrating rate ($\frac{dC}{dt}$). In MDC however, the interfacial supersaturation rate differs from the concentrating rate due to temperature polarisation which can change C^*_{int} over time. As such, a modified supersaturation rate was developed in this work to provide a more accurate description of system metastability. Substitution of R' into Eq. (19) and linearising yields:

$$ln(R') = m[ln(ln\ S_{int})] + ln\ (k) \tag{21}$$

Hence, a plot of $ln(R')$ versus $ln(ln\ S_{int})$ provides a linear trend, from which the nucleation constants k and m can be derived.

The primary nucleation mechanism is dependent on whether a reduction in the activation energy barrier required for nucleation in the system can be achieved. For a homogeneous nucleation mechanism, the critical Gibbs free energy required for nucleation (ΔG^*) is [3,27]:

$$\Delta G^* = \frac{16\pi}{3}\frac{\gamma^3 v^2}{(k_B T)^2 ln^2\ S} \tag{22}$$

At a constant temperature, this energy barrier is reduced by increasing the supersaturation level of the system. The energy barrier can also be reduced by the introduction of a foreign substrate (such as the membrane surface) which would decrease the effective interfacial energy such that heterogeneous nucleation takes place at a lower activation energy [3]:

$$\Delta G^*(\gamma_{eff}) < \Delta G^*(\gamma) = \Delta G^*_{het} < \Delta G^*_{hom} \tag{23}$$

where γ_{eff} is the effective interfacial energy and ΔG^*_{het} and ΔG^*_{hom} are the critical energy barriers for heterogeneous and homogeneous nucleation, respectively. By considering that the induction time is inversely proportional to the nucleation rate, the primary nucleation mechanism can be determined from induction time measurements. Hence, by substituting into Eq. (4) and linearising:

$$\ln(t_{ind}) = -lnA + \frac{B}{ln^2 S_{int}} \tag{24}$$

A plot of $\ln(t_{ind})$ against $ln^{-2}S_{int}$ therefore yields a straight line with a gradient of B. From Eq. (5) it can be deduced that at constant temperature, lower gradients, i.e., B values, show a tendency towards heterogeneous nucleation by reducing γ [3,27,28].

3. Results and discussion

3.1. Reynolds number determines flux and the onset of nucleation

Solute convection toward the membrane surface in direct contact MDC is a balance between the vapour pressure gradient fixed by the transmembrane temperature difference (ΔT), and the boundary layer characteristics prescribed by the hydrodynamic conditions [29,30]. Since permeate flux is an indication of the rate of solute convection, the effects of ΔT and Re on permeate flux were independently examined (Fig. 1a). Comparison at the same time interval evidenced that an increase in ΔT from 15 to 25 °C, raised permeate flux from 7.0 to 23.4 kg m^{-2} h^{-1} (Re 1300). Similarly, an increase in Re from 1300 to 2050 at a fixed ΔT (25 °C shown here to illustrate), yielded an enhancement in permeate flux from 23.4 to 37.3 kg m^{-2} h^{-1}. While increasing ΔT enhances the vapour-pressure driving force, higher Re promotes boundary-layer mixing therefore improving heat and mass transfer conditions. Hence, both variables increase the rate of solute transport to the membrane interface.

Bulk nucleation was consistently determined for each condition by an increase in turbidity (Fig. 1b). The onset of bulk nucleation was observed sooner when ΔT was increased. Turbidity peaks indicating the onset of nucleation were noted at 98, 65 and 45 min for 15, 20 and 25 °C respectively, when Re was fixed to 1300. An increase in Re at a fixed ΔT of 25 °C also decreased the time at which bulk nucleation was observed from 45 to 37 and 31 min for Re 1300, 1750 and 2050 respectively. The onset of a rapid flux decline, which authors have previously used to indirectly infer nucleation, showed a lag time of 72 min relative to the turbidity peak (red dashed line: Re 1300; ΔT 15 °C) [12]. This emphasises how such methodologies do not allow for the direct detection of induction time as suggested by Horseman et al. [2] and therefore cannot be used for the determination of nucleation kinetics within MDC.

3.2. Reynolds number determines the kinetics of nucleation and growth

The interfacial supersaturation rate (R') provides an analogy to the nucleation rate [23], while the interfacial supersaturation level (S_{int}) gives a measure of the metastable zone width (MSZW) within the boundary layer at induction (Fig. 2). At each fixed ΔT, an increase in Re corresponded to an increase in the interfacial supersaturation achieved at the time induction was measured by turbidimetry in the bulk solution. Consequently, this provides the first direct evidence that the boundary layer conditions set by Re directly determine the nucleation kinetics of the bulk crystal phase. This can be explained by the modification of mass

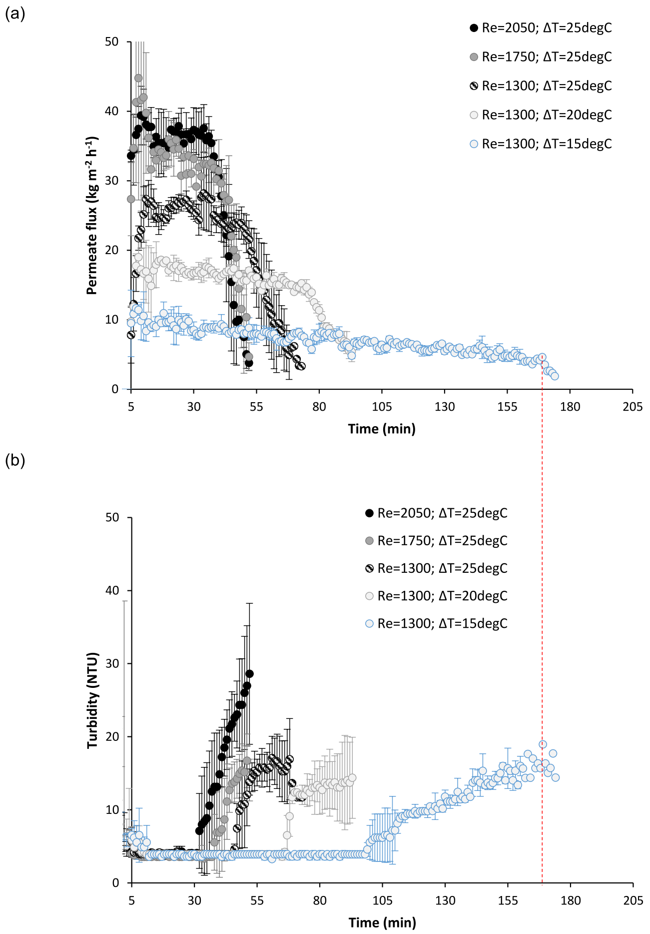

Fig. 1. Illustration of how temperature difference (ΔT 15–25 °C) and Reynolds number (Re 1300–2050) alter the water vapour flux (a), and the onset of bulk nucleation, which is identified with turbidimetry. Dotted line indicates onset of bulk nucleation based on the conventional approach of using the flux inflection point to infer induction. Data repeated in triplicate.

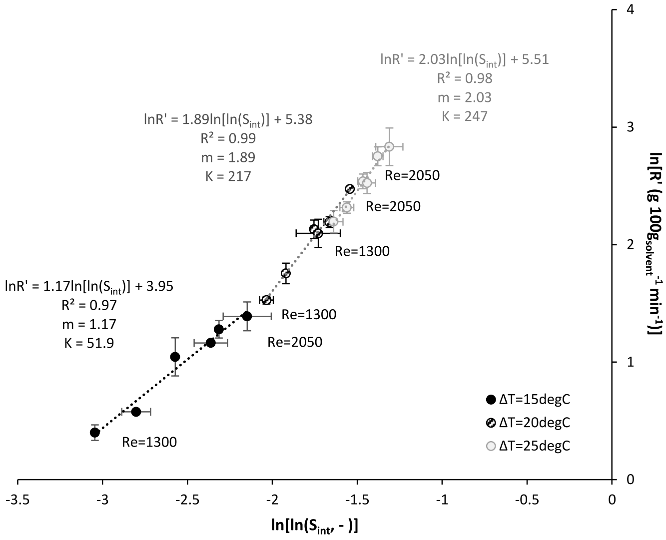

Fig. 2. Characterisation of nucleation kinetics based on bulk nucleation using the modified power-law relationship proposed by Sangwal (2009). The relationship between interfacial supersaturation rate (R') and metastable zone width (MSZW, $\ln(S_{int})$) enables determination of the apparent nucleation order (m) and nucleation constant (K) for the system. Experimental conditions: ΔT 15-25 °C, Re 1300–2050, feed temperature 60 °C. Data repeated in triplicate.

and heat transfer processes instigated by an increase in Re which raises R' due to the adjustment in permeate flux (Fig. 1a). For the same ΔT, an increase in Re therefore introduces higher nucleation rates. A power-law dependency between R' and MSZW was determined for each ΔT. This characteristically linear response was observed following an increase in Re with each ΔT and demonstrates that the interfacial supersaturation concentration set within the boundary layer by Re directly corresponds to the nucleation rate measured in the bulk solution. The gradient of the line represents the nucleation order (Eq. (21)). At a ΔT of 15 °C, a low nucleation order (<5 [31]) was observed [$m = 1.17 < 5$ (dimensionless)] indicating strong diffusive interactions between the solute (NaCl) and solvent (water), which promoted the aggregation and growth of nuclei near the membrane interface. These interactions were facilitated by the high interfacial NaCl concentration, which reduced the distance between the solute molecules and can favour cluster formation [23,31]. A comparable response was identified for ΔT of 20 and 25 °C, with higher nucleation orders of 1.89 and 2.03 observed respectively. While an increase in Re raised the interfacial supersaturation level considerably, which is the driving force for nucleation [23], bulk nucleation did not proceed until the bulk solution approached saturation ($C/C^* \sim 1$) irrespective of the ΔT or Re applied (Fig. 3). We therefore suggest that while the nucleation rate is fixed by the interfacial supersaturation concentration, a thermodynamically stable crystal phase cannot be sustained until the bulk solution achieves saturation. A co-dependency is therefore established between boundary layer and bulk solution, where nucleation is dependent on the interfacial boundary layer condition, while the formation of a stable crystal phase is dependent on the bulk solution. This implies that induction may proceed somewhere within the upper fluidised region of the boundary layer or approaching the bulk solution where the net flux of nuclei formed within the supersaturated boundary layer can grow into a thermodynamically viable crystal phase once the bulk solution approaches saturation. The small increase in bulk saturation from 0.996 ± 0.002 to 1.006 ± 0.005 following an increase in ΔT from 15 to 25 °C can be attributed to a rise in metastability of solution which is in accordance with CNT, but the extent of supersaturation in the bulk at induction is insufficient to independently overcome the energy barrier for nucleation.

Distinct morphologies were observed in crystals recovered from the bulk solution when exposed to different hydrodynamic conditions (Fig. 4). At Re 1300 (ΔT 25 °C), a characteristic cubic structure was formed, but many crystals contained hollows within which a stepped surface structure was observed (Fig. 4a). This form is referred to as a

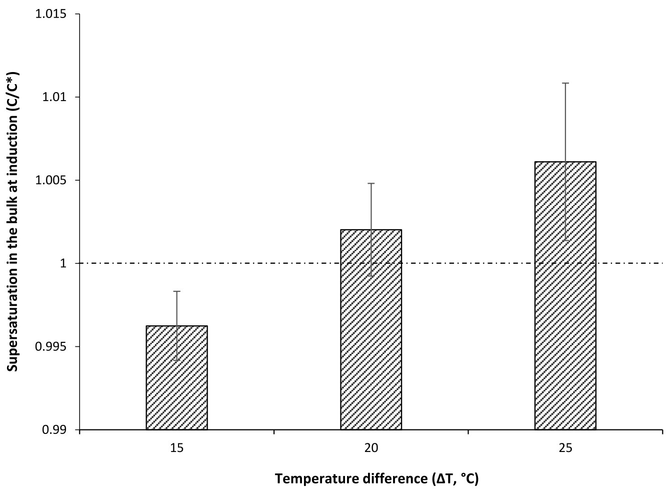

Fig. 3. Extent of supersaturation achieved in bulk solution at induction for the bulk crystal phase. For each ΔT, saturation approaches a $C/C^* \sim 1$ (dashed line). The average and error bars for each ΔT represent saturation data from each Re for that temperature difference and were repeated in triplicate (n = 21). Experimental conditions: ΔT 15-25 °C, Re 1300–2050, feed temperature 60 °C.

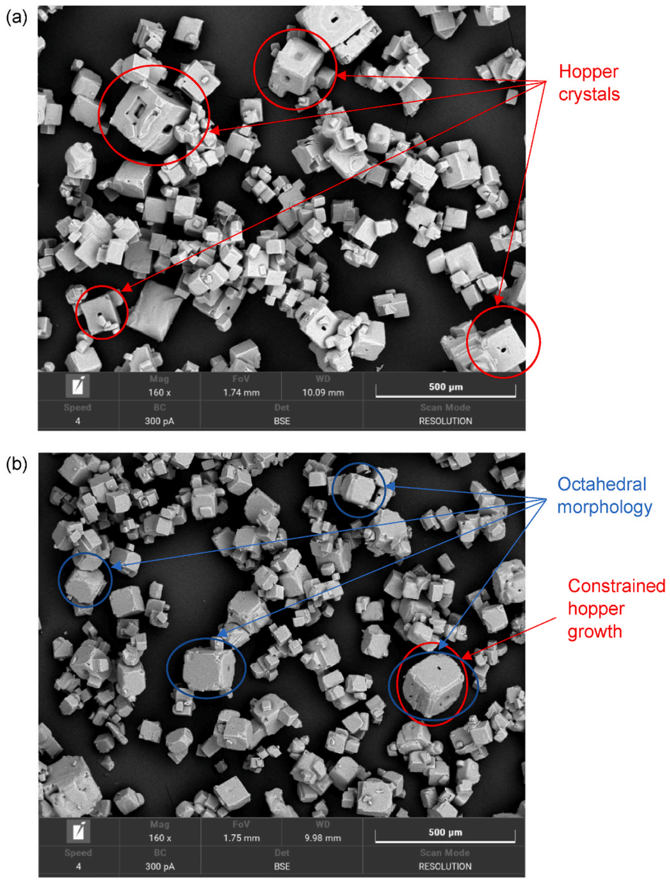

Fig. 4. High-resolution scanning electron microscopy (SEM) images of crystals collected 10 min after the onset of bulk nucleation: (a) *Re* 1300; and (b) *Re* 2050. Experimental conditions: ΔT 25 °C, feed temperature 60 °C.

hollow, or skeletal, cubic hopper crystal [32,33]. Hopper cube morphology occurs in conditions of relatively low supersaturation, as this can introduce a heterogeneous distribution of supersaturation at the crystal faces [33,34]. Consequently, higher supersaturation levels occur at the edges and corners compared to the crystal faces. This promotes crystal growth preferentially at the edges and corners, resulting in the formation of hollows [32,33]. Aquilano et al. [35] observed that an increase in supersaturation rate can shift crystal morphology from cubic to the co-existence of octahedral and cubic forms. The onset of the octahedral form was observed in this study for *Re* 2050 (ΔT 25 °C) where the loss of faces around the edges and corners of the crystal can be accounted for by the kinetic competition between cubic and octahedral forms (Fig. 4b). Development of the hollow hopper structure was also constrained at *Re* 2050. This can be explained by the increased mixing which promotes solute diffusion by forced convection and is sufficient to overcome diffusion-controlled growth [36]. Increasing supersaturation rate through *Re* is therefore shown to shift both the morphology and quality of the crystal product, which can be of critical importance for downstream application.

3.3. Comparison of surface scaling and bulk crystallisation kinetics

The nucleation and growth of scale is presumed to follow classical nucleation theory (CNT) [26,12]. Accordingly, the nucleation kinetics of scaling were characterised at different *Re* and compared to those of bulk nucleation at an equivalent ΔT of 25 °C (Fig. 5). Nucleation kinetics were derived at the onset of scaling (the first measurable crystal growth formed on the membrane at induction). A linear correlation between supersaturation rate and supersaturation was evidenced when analysing

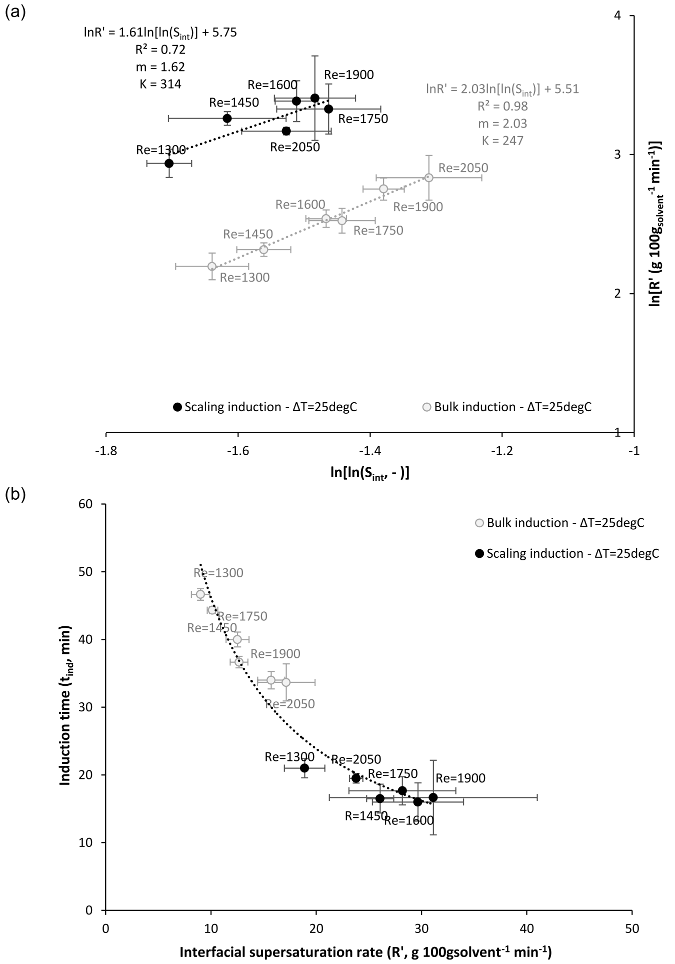

Fig. 5. Characterisation of nucleation kinetics for scaling based on the modified power-law relationship proposed by Sangwal (2009). The relationship between interfacial supersaturation rate (R') and metastable zone width (MSZW, $\ln(S_{int})$) enables determination of the apparent nucleation order (m) and nucleation constant (K) for the system. Bulk nucleation data is provided for comparison: (a) supersaturation versus supersaturation rate; and (b) interfacial supersaturation rate versus induction time. Experimental conditions: ΔT 25 °C, *Re* 1300–2050, feed temperature 60 °C. The dashed-line in (b) represents a power-law fit of induction time across bulk and scaling data. Data repeated in triplicate.

scaling kinetics based on the modified power-law relationship proposed by Sangwal [23]. This was comparable to the kinetic relationship established for bulk nucleation, but the nucleation rate (an analogy to $\ln R'$ at the onset of scaling) was considerably higher for scaling. A higher supersaturation rate is established in the boundary layer compared to the bulk due to concentration and temperature polarisation which increases supersaturation locally. This is emphasised by the reduced nucleation order that implies greater solute-solvent interactions exist [23,31] at the onset of scaling which subsequently increases nucleation rate. At ΔT 25 °C, scaling was consistently observed for each *Re* before induction of the bulk crystal phase occurred, where the inception of scaling corresponded to a highly supersaturated boundary layer and an undersaturated bulk solution (C/C^* 0.973 ± 0.006) which emphasises that unlike bulk nucleation, scaling is not dependent on the bulk solution for the formation of a stable crystal phase.

Induction time is the time interval between reaching saturation and the time at which nucleation occurs, and is therefore a measure of the metastability of solution [37]. For bulk nucleation, an increase in *Re* shortened induction time and increased nucleation rate (R') (Fig. 6). This corresponds to homogeneous primary nucleation where induction

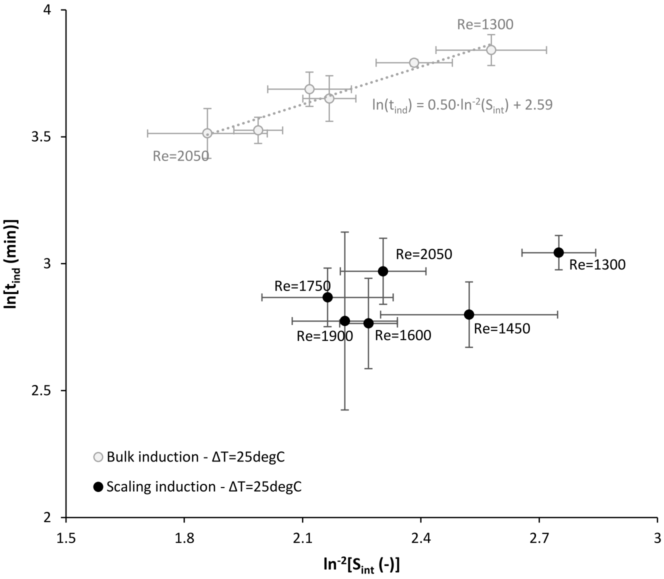

Fig. 6. Evaluation of primary nucleation mechanism(s) for scaling. The relationship between induction time and metastable zone width (MSZW, $\ln(S_{int})$) is more difficult to discern for scaling due to polarisation. Bulk nucleation data is provided for comparison. Experimental conditions: ΔT 25 °C, *Re* 1300–2050, feed temperature 60 °C. Data repeated in triplicate.

time is recognised to be inversely proportional to nucleation rate. Consequently, much shorter induction times were recorded for scaling, which corresponded to higher nucleation rates, and can be accounted for by the higher supersaturation level achieved at induction for scaling (Fig. 6). The inverse relationship between induction time and supersaturation conforms with classical nucleation theory where higher supersaturation levels increase the likelihood of nucleation [28,37]. Increasing *Re* reduced induction time for bulk nucleation by raising the rate of solute transport to the interface therefore increasing interfacial supersaturation (S_{int}), where the gradient of the slope (0.50) represents the relative interfacial free energy which is the main contributor to the nucleation barrier [27]. While scaling nucleation rate was also observed to increase with a reduction in induction time, a reduction in induction time did not correspond to an increased supersaturation level at induction for scaling following an increase in *Re* (Fig. 6). Therefore, while the interfacial supersaturation established within the boundary layer by *Re* directly regulates nucleation rate in the bulk solution, other local transport phenomena may be involved in defining the kinetics of scaling.

Microscopic examination emphasised distinct crystal growth mechanisms for the scale formed (Fig. 7). The dendritic (branched) morphology differed from the growth of singular cubic hopper crystals observed in the bulk solution (Fig. 4). This dendritic interconnected hopper growth profile is characteristic of crystal growth within highly-supersaturated and confined homogeneous solutions [38], that can be considered similar to the pore structure within the stagnant interfacial region established in MDC. Highly supersaturated regions promote a shift from diffusion limited to surface-integration limited crystal growth, which encourages creation of surface area as interconnected cubes formed by secondary nucleation from the central nucleus. The polyhedral growth evidenced at *Re* 1300 is consistent with growth patterns observed in highly supersaturated and confined conditions in other environments, where an inversely proportional relationship exists between the size of the cubes in the branches and the initial supersaturation at which they are formed [34,38]. Consequently, the interconnected cubes comprising the branches were much smaller in size for *Re* 2050, resulting in a more layered, vicinal surface with enhanced branching (more twigs). While several authors have proposed a mechanism for bulk crystal formation where scaling firstly occurs, and is followed by the detachment of crystals from the membrane into the bulk solution once a critical shear stress is achieved [3,5,8], the contrasting morphologies of crystals formed in the bulk and at the membrane in this study, infer that the two crystal growth mechanisms are distinct.

3.4. *Relating scaling to boundary-layer phenomena by using solute mass transport*

Membrane surface coverage was characterised at the induction time for the bulk crystal phase, to determine the extent of membrane scaling prior to bulk nucleation (Fig. 8). At *ΔT* 15 °C, negligible scaling was observed prior to the formation of the bulk crystal phase, independent of the *Re* used. The negligible effect of scaling by adhesive growth (classical scaling) or deposition was highlighted by the consistent flux observed both before and after induction in the bulk (Fig. 1), where flux was sustained for over 169 min before a significant 'stage 3' flux decline was observed (71 min after bulk induction was achieved). Despite negligible scaling being observed up to bulk nucleation, bulk nucleation was consistently demonstrated at each *Re*, to support the hypothesis that the formation of the bulk crystal phase is not critically dependent on first forming a crystalline phase at the membrane. A small increase in scaling was observed when *ΔT* was raised from 15 to 20 °C within the *Re* range 1450–1900. However, surface coverage was most pronounced within the same *Re* range, when ΔT increased to 25 °C. An increase in ΔT improves heat and mass transfer, while the lower permeate temperature used to raise *ΔT* to 25 °C, also reduces the solubility constant due to an increase in temperature polarisation. This increases the local supersaturation and supersaturation rate, which can raise the probability for localised nucleation of scale despite the relatively flat solubility-temperature dependency of NaCl.

At a *ΔT* of 25 °C, the extent of membrane scaling at bulk induction increased from 29 × 10^{-6} m^2 at *Re* 1350 to a maximum of 231 × 10^{-6} m^2 at *Re* 1750, after which a further increase in *Re* resulted in a reduction of scaling (Fig. 8). It has previously been suggested, based on modelling, that an increase in *Re* may reduce the likelihood of scaling by lowering the solute residence time at the membrane [12]. However, modelling cannot presently account for how modifying boundary layer properties by an increase in *Re* will adjust the supersaturation level at induction as this is kinetically dependent, and is thus determined by the supersaturation rate established for each specific *Re*. Furthermore, the extent of supersaturation will also alter the concentration dependent diffusion coefficient, which is critical to solute backtransport, and hence will determine the extent of interfacial concentration polarisation that will be achieved. Consequently, supersaturation (metastable zone width) was characterised and used to determine interfacial boundary layer properties that may also influence the probability for scaling.

An increase in *Re* reduced boundary layer thickness, but this improved mass and heat transfer processes within the boundary layer which enhanced the interfacial solute concentration at higher *Re* (Fig. 9a). To illustrate, at the lowest *Re* of 1300 where the boundary layer thickness approached a maximum, the interfacial solute concentration tended toward a minimum. In contrast, interfacial solute concentration increased from 10.9 to 11.7 mol m^{-2} when *Re* was modified to 1750. The concentration polarisation coefficient is generally estimated using a diffusion coefficient that is defined based on the bulk concentration. However, at the induction time for scaling, the bulk solution is undersaturated (C/C* 0.973 ± 0.006) and since the diffusion coefficient has been shown to exhibit a strongly negative concentration dependency within supersaturated NaCl solutions [20–22], this will lead to a misrepresentation of the extent of concentration polarisation within the boundary layer. The interfacial diffusion coefficient (D_{int}) was therefore calculated from empirical data derived in supersaturated NaCl solutions (Appendix A) based on the specific interfacial solute concentration determined for each *Re* in order to revise the concentration polarisation coefficient. This demonstrated a marked reduction in the interfacial diffusion coefficient from 12.7 × 10^{-10} to 11.8 × 10^{-10} m^2

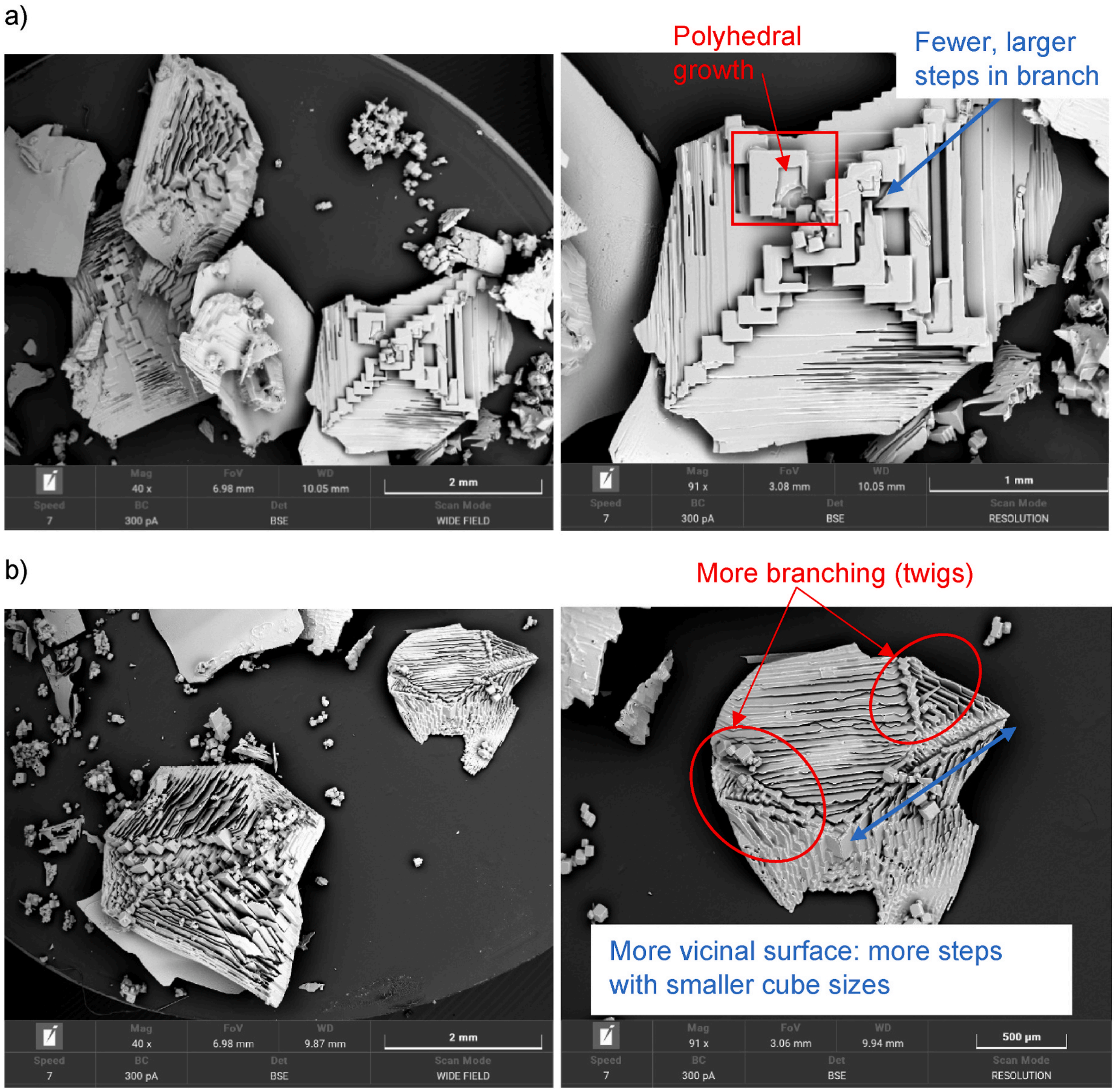

Fig. 7. High-resolution scanning electron microscopy (SEM) images of scaling formed at the membrane: (a) *Re* 1300; and (b) *Re* 2050. Experimental conditions: ΔT 25 °C, feed temperature 60 °C.

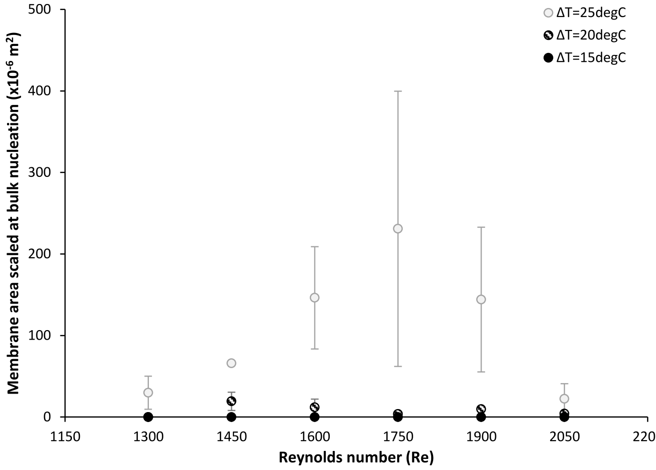

Fig. 8. Extent of scaling at the onset of bulk nucleation as determined by non-invasive digital microscopy. Experimental conditions: ΔT 15-25 °C, *Re* 1300–2050, feed temperature 60 °C. Data repeated in triplicate.

s^{-1} following an increase in *Re* from 1300 to 1750 due to the increase in solute concentration (Fig. 9a).

Concentration polarisation represents the interfacial solute concentration that develops due to the balance between the rate of solute convection toward the membrane, and the back-diffusion of solute (NaCl) from the boundary layer toward the bulk solution (Eq. (1)). Consequently, there are two factors (convection and diffusion) that will determine the extent of concentration polarisation and hence the supersaturation at induction. The revised CPC permits description of both factors and illustrates that the conventional method of CPC determination significantly underestimates interfacial concentration polarisation, but also that it is the balance between convection and diffusion that determines the extent of CPC (Fig. 9b). In this study, the revised CPC strongly correlates to the extent of scaling, where maximum scaling was observed for conditions that elicit the highest convection, and therefore the lowest interfacial diffusion which is a compounding factor in driving the interfacial solute concentration. However, higher diffusion rates are also noted to lower the critical size at which a thermodynamically stable nucleus is formed [39]. The interfacial diffusion coefficient therefore modifies the interfacial solute concentration through its role in

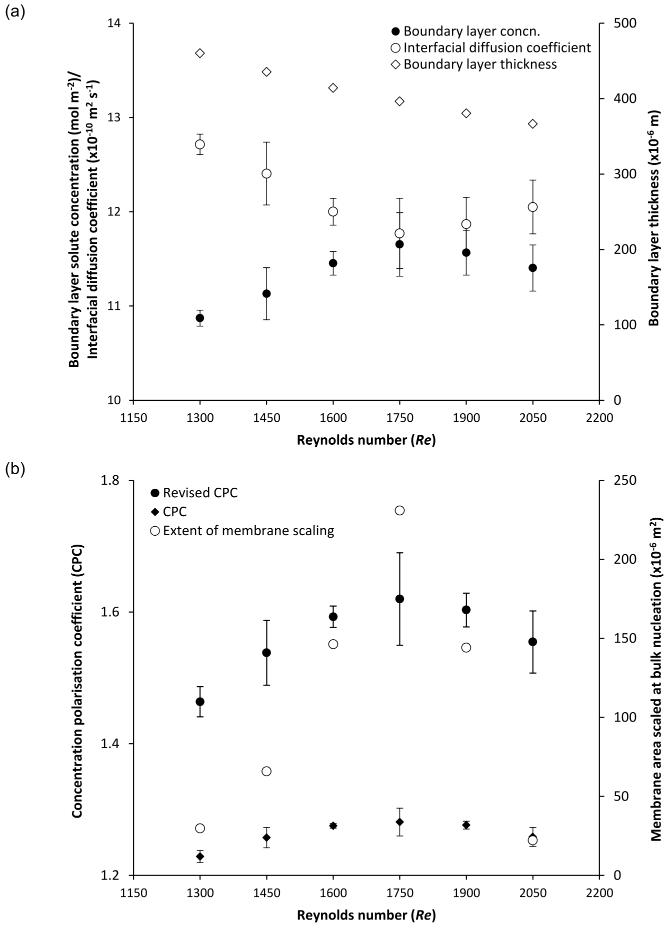

Fig. 9. An increase in *Re* reduces boundary layer thickness but the increase in mass and heat transfer increases solute concentration: (a) which has implications for the interfacial diffusion coefficient; and (b) this determines solute back transport within the boundary layer, and hence modifies the CPC. Comparison of scaling rate to the revised CPC illustrates an analogous criticality at *Re* 1750. Experimental conditions: ΔT 25 °C, feed temperature 60 °C, *Re* 1300–2050. Data repeated in triplicate.

determining solute backtransport, while simultaneously adjusting the activation energy requirement for nucleation. We propose that it is this interdependency on the interfacial properties (D_{int}) that makes the relation between interfacial supersaturation and nucleation rate more complex to describe for scaling. This is distinct from bulk crystallisation where induction is observed to be dependent on achieving saturation in the bulk solution ($C/C^* \sim 1$), providing more consistent physical properties at nucleation independent of *Re* or ΔT (Fig. 3).

The revised CPC was used to re-evaluate the interfacial supersaturation level (S_{int}) and relate this to the extent of scaling observed (Fig. 10). Whereas the conventional CPC method determined a maximum S_{int} of 1.26 (*Re* 1750, ΔT 25 °C), the revised CPC reported S_{int} up to 1.6. Scaling was only prevalent when $S \geq 1.45$, which is coincident with the threshold supersaturation level identified in the literature for the transition from cubic to hopper morphology for halite (NaCl) [38]. This morphology is comparable to the scaling determined in this study, where the hopper form leads to conditions approaching maximum crystal growth (6.5 ± 1.8 μm s^{-1} for previous research [38], which is within the same order of magnitude to that determined in this study (Appendix B)). Identification of a comparable supersaturation level for the onset of 'hopper' growth to the literature provides corroborative evidence that the revised CPC calculation is more representative of the interfacial solute concentration in MDC. This also introduces a new threshold supersaturation value below which scaling by 'hopper' growth cannot be sustained, and growth defers to a cubic form which is characterised by considerably lower growth rates. This threshold value can therefore be used to inform scaling mitigation strategies to suppress scaling in favour of crystal growth in the bulk solution. A reduction in scaling was observed once *Re* was increased from 1750 to 2050. As the velocity within the boundary layer approaches zero toward the wall, mass transport in the vicinity of where scale is formed is dominated by natural diffusion and is best described by Fick's first law of mass transport:

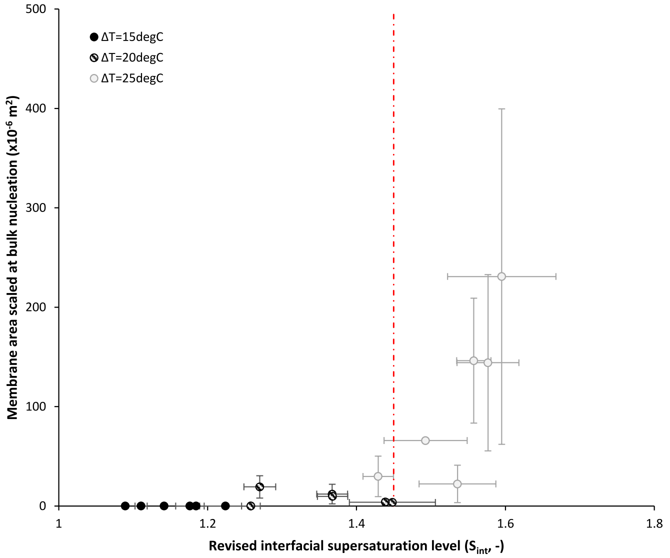

Fig. 10. The revised CPC is used to estimate the local supersaturation level, indicating a critical supersaturation threshold beyond which the scaling rate becomes significant (S 1.45, red dashed line) and is dominated by hopper crystal growth. This threshold value is equivalent to that identified in the literature as the transition from the formation of singular cubic NaCl crystals to the growth of hopper crystals characterised by series of interconnected cubes (Desarnaud, 2018). Data repeated in triplicate. (For interpretation of the references to colour in this figure legend, the reader is referred to the Web version of this article.)

$$J_{solute} = -D\frac{dC}{dx} \tag{25}$$

where J_{solute} is the diffusional flux of solute from the interface to the bulk solution, and $\frac{dC}{dx}$ is the concentration gradient which increases as the boundary-layer thickness decreases (dx). The reduction in boundary layer thickness with an increase in *Re* may therefore have improved solute migration from the membrane to the bulk solution by increasing $\frac{dC}{dx}$, complemented by an increase in velocity of the fluidised region of the boundary layer when approaching transitional flow. Importantly, the scaling rate could be related to the revised CPC and supersaturation threshold for each *Re* and ΔT studied, evidencing that the approach to mitigate scaling is valid for a wide range of conditions.

4. Conclusions

In this study, Reynolds number is demonstrated to directly inform the kinetics of nucleation and growth for scaling and the bulk crystal phase. A modified power law relation between nucleation rate and supersaturation was introduced to characterise primary nucleation which was made possible by the first direct measurements of induction time for scaling and bulk crystallisation in MDC. Higher Reynolds numbers increased mass and heat transfer processes which raised the supersaturation rate (an analogy to nucleation rate) and shortened induction time. The interfacial conditions correlated favourably to classical nucleation theory for bulk crystallisation, which evidenced for the first time that it is the supersaturation level set within the boundary layer which controls primary nucleation of the crystal phase that is found in the bulk solution. However, it was also demonstrated that to establish a thermodynamically stable crystal phase, the bulk solution must have achieved saturation. This is important as previous studies have assumed that the primary role of Reynolds number is to provide the critical shear stress required to detach crystals from the membrane. The dependence of bulk nucleation on the bulk solution approaching a set saturation value implies that induction occurs at the interface between the boundary layer and bulk solution following migration of nuclei formed within the interfacial region, where they can establish and grow within the saturated solution. Consequently, this provides evidence that bulk crystals are not initially formed at the membrane which is distinct from what was previously assumed. The description of supersaturation rate developed within this study can therefore be used to control nucleation kinetics in membrane systems, where an increase in Reynolds number was shown to raise nucleation rate. While scaling nucleation rate was also observed to be dependent on the interfacial supersaturation level, which indicates that high Reynolds numbers are in fact detrimental to scaling, the modification of scaling kinetics was not directly related to an increase in Reynolds number. The diffusion coefficient was modified to adjust interfacial solute concentration and provide closer corollary between interfacial supersaturation and scaling rate, confirming that scaling is dependent on boundary layer properties and not those of the bulk solution. A threshold supersaturation value was subsequently identified above which scaling proceeds via ‘hopper’ growth in which maximum growth rates are observed. This threshold value, together with the revised concentration polarisation coefficient provide a framework with which to mitigate scaling using Reynolds number. While the formation of scaling and bulk crystals are seemingly distinct, complimentary strategies to mitigate scaling and control nucleation rate can be developed using Reynolds number, where exploitation of this dimensionless quantity can ensure replication across systems of various configuration and scale provided fully developed laminar flow is established.

Author statement

A. Jikazana: Conceptualization; Data curation; Formal analysis; Investigation; Methodology; Roles/Writing - original draft;

P. Campo: Writing - review & editing.

E. McAdam: Conceptualization; Data curation; Formal analysis; Funding acquisition; Investigation; Methodology; Project administration; Supervision; Writing - review & editing.

Declaration of competing interest

The authors declare that they have no known competing financial interests or personal relationships that could have appeared to influence the work reported in this paper.

Data availability

The data underlying this paper can be accessed through the following link: 10.17862/cranfield.rd.23504427.

Acknowledgements

This research was financially supported by European Research Council Starting Grant 714080, ‘*Sustainable chemical alternatives for reuse in the circular economy*’ (SCARCE). The data underlying this paper can be accessed through the following link: 10.17862/cranfield.rd.23504427.

Appendix A. Diffusion in supersaturated solution

In membrane distillation crystallisation (MDC), the solute back transport through the stagnant boundary layer is diffusive [1]. The rate of this diffusive solute flow is dependent on the diffusion coefficient, which is in important parameter in the calculation of the concentration polarisation coefficient (CPC). To improve the precision of this parameter in the revised-CPC approach, the diffusion coefficient as a function of (temperature independent) molality was derived based on the literature data from Rard and Miller (1979) as well as that of Chang and Myerson (1985) (Figure A1). According to Zimmerman et al. (2015), after the observed maximum, the diffusion coefficient is expected decrease monotonically with further increases in molality. Based on this assumption, a linear trendline was fitted using the four available literature data points of highest molality. The resultant equation was then applied to determine the interfacial diffusion coefficient at experimental molalities above 6 mol kg_{water}^{-1}.

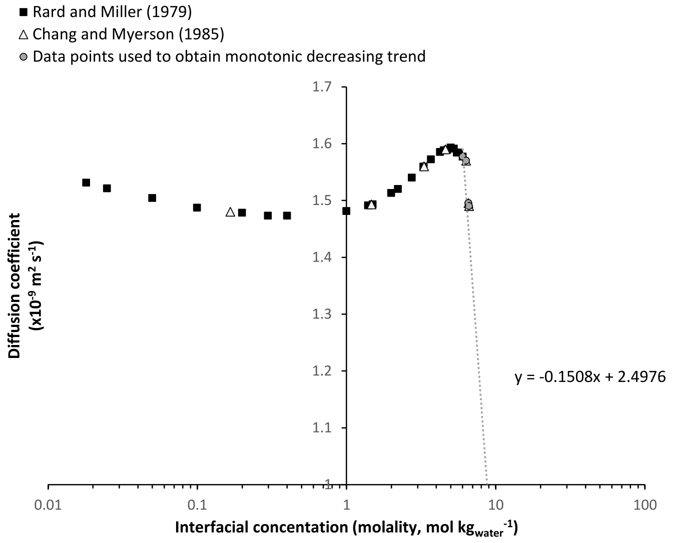

Fig. A1. Determination of diffusion coefficient based on interfacial concentration (molality). Figure shows literature data used to derive diffusion coefficients with extrapolation based on assumption of monotonic decrease in molality within supersaturated conditions (Zimmerman et al., 2015).

Appendix B. Characterisation of scaling through imaging

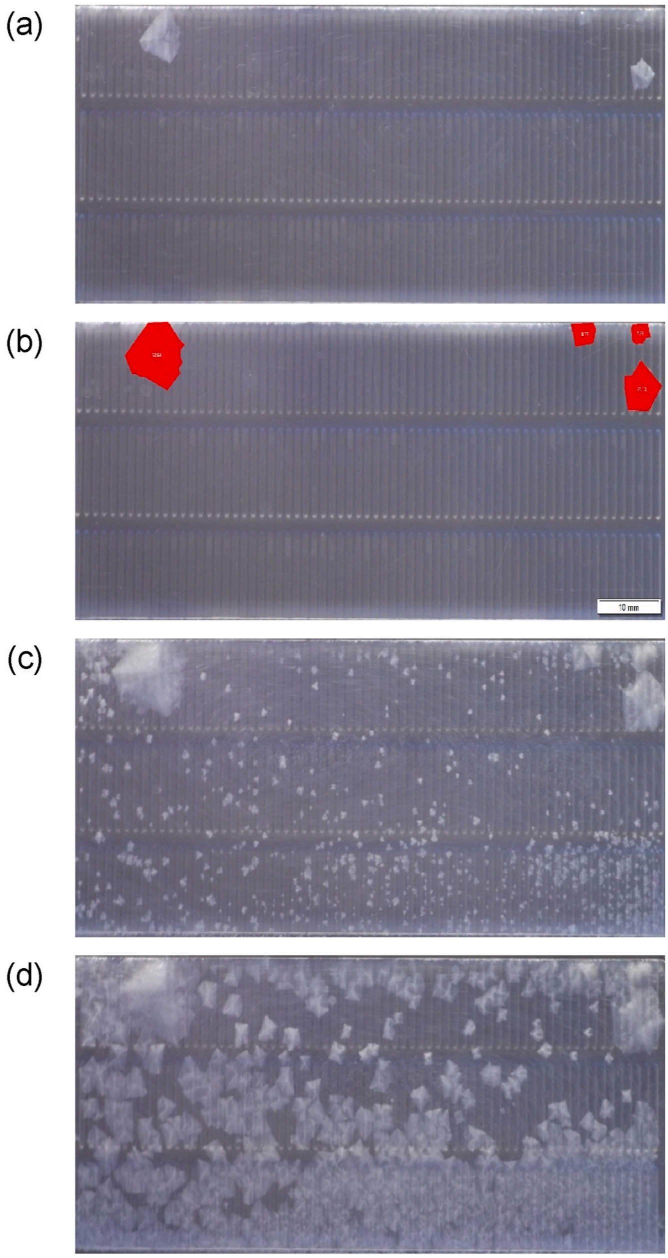

Fig. B1. Example digital image time series: (a) following the commencement of scaling, several early crystals and formed that quickly grow due to the excess of supersaturation in the boundary layer; (b) illustration of surface area measurement following further growth of early formed individual crystals. Scale bar presented (10 mm); (c) shortly after bulk induction, the number density of crystals increases on the membrane surface; (d) after a 5-min elapse from (c), the crystal phase exhibits significant growth due to the progressive increase in system supersaturation provided by continued concentration of the feed solution, coupled with the enriched supersaturated state within the boundary layer.

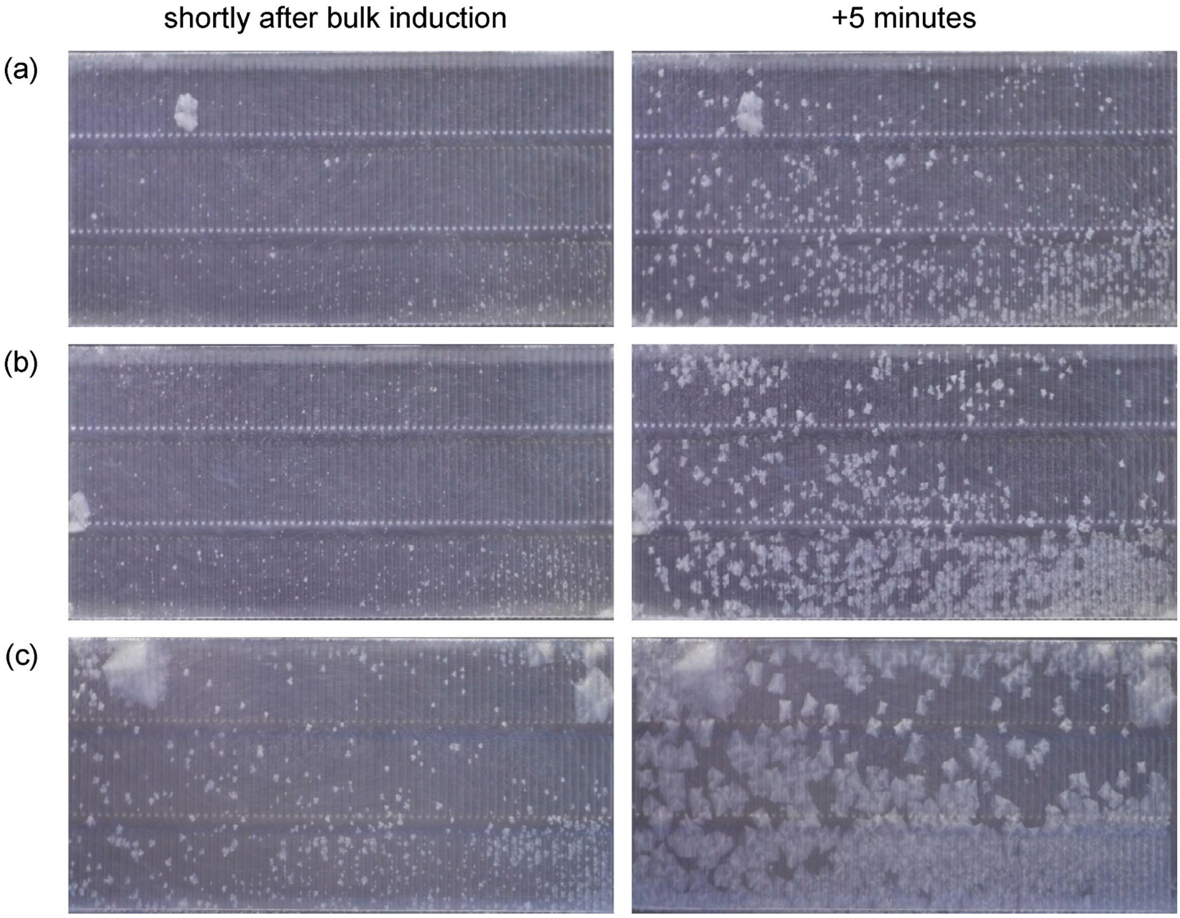

Fig. B2. Digital imaging of membrane surface showing scaling shortly after induction, and images from the same membrane sample taken 5 min later to illustrate how fast crystal growth proceeds on the membrane due to the elevated supersaturation within the boundary layer. The growth rate of individual crystals on the membrane is exacerbated by an increase in temperature difference due to the increase in supersaturation rate: (a) 15 °C; (b) 20 °C; and (c) 25 °C.

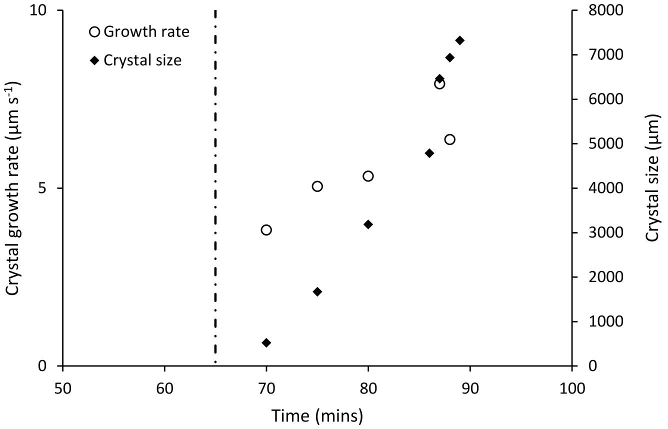

Fig. B3. An illustration of crystal growth for scaling through image analysis of a single crystal formed at induction (dashed line, 65 min). As the feed solution continues to concentrate, the system supersaturation increases, which is the driving force for crystal growth. Consequently, the crystal growth rate increases with time. The interfacial crystal growth rate is exacerbated by the elevated supersaturation in the boundary layer which leads to the production of large crystals. The crystal growth rates are comparable to those observed for hopper growth of halite in the literature [38].

References

[1] Y. Choi, G. Naidu, L.D. Nghiem, S. Lee, S. Vigneswaran, Membrane distillation crystallization for brine mining and zero liquid discharge: opportunities, challenges, and recent progress, Environ. Sci. Water Res. Technol. 5 (2019) 1202–1221.

[2] T. Horseman, Y. Yin, K.S. Christie, Z. Wang, T. Tong, S. Lin, Wetting, scaling, and fouling in membrane distillation: state-of-the-art insights on fundamental mechanisms and mitigation strategies, ACS ES&T Eng. 1 (2021) 117–140.

[3] G. Di Profio, E. Curcio, E. Drioli, Supersaturation control and heterogeneous nucleation in membrane crystallizers: facts and perspectives, Ind. Eng. Chem. Res. 49 (2010) 11878–11889.

[4] C. Charcosset, R. Kieffer, D. Mangin, F. Puel, Coupling between membrane processes and crystallization operations, Ind. Eng. Chem. Res. 49 (2010) 5489–5495.

[5] M.C. Sparenberg, S. Chergaoui, V. Sang Sefidi, P. Luis, Crystallization control via membrane distillation-crystallization: a review, Desalination 519 (2022), 115315.

[6] Y.N. Nariyoshi, C.E. Pantoja, M.M. Seckler, Y.N. Nariyoshi, C.E. Pantoja, M. M. Seckler, Evaluation of sodium chloride crystallization in membrane distillation

crystallization applied to water desalination, Braz. J. Chem. Eng. 33 (2016) 675–690.

[7] E. Chabanon, D. Mangin, C. Charcosset, Membranes and crystallization processes: state of the art and prospects, J. Membr. Sci. 509 (2016) 57–67.

[8] X. Jiang, et al., Interface-based crystal particle autoselection via membrane crystallization: from scaling to process control, AIChE J. 65 (2019) 723–733.

[9] A. Alkhatib, M.A. Ayari, A.H. Hawari, Fouling mitigation strategies for different foulants in membrane distillation, Chem. Eng. Process. - Process Intensif. 167 (2021), 108517.

[10] Y. Shin, J. Sohn, Mechanisms for scale formation in simultaneous membrane distillation crystallization: effect of flow rate, J. Ind. Eng. Chem. 35 (2016) 318–324.

[11] F. Edwie, T.S. Chung, Development of simultaneous membrane distillation-crystallization (SMDC) technology for treatment of saturated brine, Chem. Eng. Sci. 98 (2013) 160–172.

[12] D.M. Warsinger, E.W. Tow, J. Swaminathan, J.H. Lienhard V, Theoretical framework for predicting inorganic fouling in membrane distillation and experimental validation with calcium sulfate, J. Membr. Sci. 528 (2017) 381–390.

[13] A. Borissova, Driving force of crystallization based on diffusion in the boundary and the integration layers, Chem. Eng. Technol. 42 (2019) 661–668.

[14] D.M. Warsinger, et al., Effect of filtration and particulate fouling in membrane distillation, Int. Desalin. Assoc. (2015), 0–14.

[15] J. Kim, J. Kim, S. Hong, Recovery of water and minerals from shale gas produced water by membrane distillation crystallization, Water Res. 129 (2018) 447–459.

[16] R.S. Harner, R.J. Ressler, R.L. Briggs, J.E. Hitt, P.A. Larsen, T.C. Frank, Use of a fiber-optic turbidity probe to monitor and control commercial-scale unseeded batch crystallizations, Org. Process Res. Dev. 13 (2009) 114–124.

[17] A. Ouda, Y. Bajón Fernández, E. McAdam, Modifying supersaturation rate with membrane area to volume ratio: scaling reduction and improved crystal growth in membrane distillation crystallisation, J. Membr. Sci. 683 (2023), 121838.

[18] X. Jiang, D. Lu, W. Xiao, X. Ruan, J. Fang, G. He, Membrane assisted cooling crystallization: process model, nucleation, metastable zone, and crystal size distribution, AIChE J. 62 (2016) 829–841.

[19] O.R. Lokare, R.D. Vidic, Impact of operating conditions on measured and predicted concentration polarization in membrane distillation, Environ. Sci. Technol. 53 (2019) 11869–11876.

[20] Y.C. Chang, A.S. Myerson, The diffusivity of potassium chloride and sodium chloride in concentrated, saturated, and supersaturated aqueous solutions, AIChE J. 31 (1985) 890–894.

[21] J.A. Rard, D.G. Miller, The mutual diffusion coefficients of NaCI-H20 and CaCl2-H2O at 25oC from Rayleigh interferometry, J. Solut. Chem. 8 (1979).

[22] N.E.R. Zimmermann, B. Vorselaars, D. Quigley, B. Peters, Nucleation of NaCl from aqueous solution: critical sizes, ion-attachment kinetics, and rates, J. Am. Chem. Soc. 137 (2015) 13352–13361.

[23] K. Sangwal, A novel self-consistent Nývlt-like equation for metastable zone width determined by the polythermal method, Cryst. Res. Technol. 44 (2009) 231–247.

[24] A. Alkhudhiri, N. Darwish, N. Hilal, Membrane distillation: a comprehensive review, Desalination 287 (2012) 2–18.

[25] A. Lewis, M.M. Seckler, H. Kramer, G. van Rosmalen, Industrial Crystallization, Cambridge University Press, Cambridge, 2015.

[26] X. Jiang, X. Ruan, W. Xiao, D. Lu, G. He, A novel membrane distillation response technology for nucleation detection, metastable zone width measurement and analysis, Chem. Eng. Sci. 134 (2015) 671–680.

[27] G. Zeng, H. Li, S. Huang, X. Wang, J. Chen, Determination of metastable zone width and the primary nucleation kinetics of sodium sulfate, Theor. Found. Chem. Eng. 49 (2015) 869–876.

[28] Z. Guo, L. Li, W. Han, J. Li, B. Wang, Y. Xiao, Interpretation of the microwave effect on induction time during CaSO4 primary nucleation by a cluster coagulation model, J. Cryst. Growth 475 (2017) 220–231.

[29] M. Gryta, Effectiveness of water desalination by membrane distillation process, Membranes 2 (2012) 415–429.

[30] C.M. Tun, et al., Membrane distillation crystallization of concentrated salts - flux and crystal formation, J. Membr. Sci. 257 (2005) 144–155.

[31] C. Devos, T. Van Gerven, S. Kuhn, A review of experimental methods for nucleation rate determination in large-volume batch and microfluidic crystallization, Cryst. Growth Des. 21 (2021) 2541–2565.

[32] I. Sunagawa, Growth and morphology of crystals, Forma 14 (Jun. 1999) 147–166.

[33] D. Pettit, P. Fontana, Comparison of sodium chloride hopper cubes grown under microgravity and terrestrial conditions, npj Microgravity 5 (2019) 1–7.

[34] S. Sarig, F. Tartakovsky, Crystal habit modifiers, J. Cryst. Growth 28 (1975) 300–305.

[35] D. Aquilano, L. Pastero, M. Bruno, M. Rubbo, {1 0 0} and {1 1 1} forms of the NaCl crystals coexisting in growth from pure aqueous solution, J. Cryst. Growth 311 (2009) 399–403.

[36] W.R. Wilcox, Transport phenomena in crystal growth from solution, Prog. Cryst. Growth Char. Mater. 26 (1993) 153–194.

[37] D. Kashchiev, G.M. Van Rosmalen, Review: nucleation in solutions revisited, Cryst. Res. Technol. 38 (2003) 555–574.

[38] J. Desarnaud, H. Derluyn, J. Carmeliet, D. Bonn, N. Shahidzadeh, Hopper growth of salt crystals, J. Phys. Chem. Lett. 9 (2018) 2961–2966.

[39] X. Dou, H. Huang, X. Wang, Q. Lin, J. Li, Y. Zhang, Y. Han, Collision dependent silver nucleation regulated by chemical diffusion and reaction, Chem. Eng. Sci. 262 (2022), 117965.

Hydrodynamics (Reynolds number) determine scaling, nucleation and crystal growth kinetics in membrane distillation crystallisation

Jikazana, Aphiwe

2023-11-05

Jikazana A, Campo P, McAdam EJ. (2023) Hydrodynamics (Reynolds number) determine scaling, nucleation and crystal growth kinetics in membrane distillation crystallisation. Journal of Membrane Science, Volume 685, November 2023, Article number 121909

https://doi.org/10.1016/j.memsci.2023.121909